Construction and Building Materials 422 (2024) 135837

Contents lists available at ScienceDirect

Construction and Building Materials

journal homepage: www.elsevier.com/locate/conbuildmat

Stress-strain behavior of electric arc furnace slag concrete under uniaxial compression: Short- and long-term evaluation

Daniel Trento [a], Vanesa Ortega-Lopez [b], Mariano Angelo Zanini [a], Flora Faleschini [a,*]

[a] Department of Civil, Environmental and Architectural Engineering, University of Padova, Via Marzolo 9, Padova 35131, Italy
[b] Department of Civil Engineering, Escuela Politécnica Superior, University of Burgos, c/ Villadiego s/n, 09001 Burgos, Spain

ARTICLE INFO

Keywords:
Baritic concrete
Cyclic loading
Concrete damage
Slag concrete
Secant modulus
Poisson's coefficient
Stress-strain curve

ABSTRACT

This work analyzes the experimental behavior of electric arc furnace slag (EAFS) concretes in terms of full stress-strain behavior under uniaxial compression. Tests are carried out on samples cured for 28 days and for more than 6 years, representing both short- and long-term conditions. Results are discussed in terms of main mechanical strength (compressive and indirect tensile strength), deformative properties in the axial and transverse direction, i.e., secant modulus and Poisson's coefficient, stress-strain relations during the load history, damage evolution and critical stress. Furthermore, two models for predicting the stress-strain behavior of concrete under repeated cycles are shown, for both natural aggregate concrete (NAC) and EAFS concrete. Results indicate that EAFS concrete has higher compressive and tensile strength than the reference, as well as better deformative properties. The aggregates type influences the deformability of the concrete also beyond the elastic regime, both in the longitudinal and transverse direction, with a different extent depending on the applied stress. Specifically, EAFS concrete attained higher secant modulus particularly at low-stress levels, while such improvement is less pronounced at high stresses. Instead, no significant differences were recorded concerning Poisson's coefficient between NAC and EAFS concrete. The analytical models proposed hereafter well predict the experimental behavior for both concrete types.

1. Introduction

The 2030 agenda for sustainable development has been signed in September 2015 by more 150 world leaders, with the aim to reach 17 sustainable development goals before 2030 [1]. One of the main target includes a revision of waste management policy [2]; in this context, civil and infrastructure engineering sector can be considered a great consumer of recycled materials which allows reducing the amount of waste to be disposed [3]. An extensive research has been already carried out to demonstrate that concrete can safely include large amounts of construction and demolition waste (C&DW) in replacement of natural coarse aggregate [4], without losing significantly its performance both in terms of strength and durability. Many other works focused on the performance of concrete containing metallurgical slags, too. Particularly, past researches attempted to establish the behavior of concrete incorporating different slag types, including ground granulated blast furnace slag [5] and basic oxygen furnace slag [6]. However, in the attempt to increase the sustainability of the steel manufacture field, such by-products will become less abundant since electric arc furnace technology is going to replace blast furnaces, leading to growing availability of electric arc furnace slag (EAFS). This has occurred already in many countries, where EAFS has exceeded abundantly the production of other slag types, such as in Italy [7]. In fact, when steel is produced in the electric arc furnace process, it is obtained starting from 100% recycled scraps, conversely than in primary steelmaking from ores, significantly reducing energy and raw materials consumption.

EAFS properties depend on several factors mainly linked to the production process, e.g., the temperature reached in the furnace, the impurities in the refractories, the overall duration of the melting phase and the type and composition of the additions (lime and dolomite fed in the furnace), but also on scraps impurities and composition, and lastly on the slag cooling method, too [8]. However, a few common characteristics can be identified: EAFS is generally hard, black and stony-like, it displays high angularity, a rough texture and a low flakiness index. Its main application in concrete is as an aggregate: its density ranges between 3200 and 4300 kg/m^3, similarly to that of barite or basalt stones; the value of water absorption is about 0.5–4.0%, slightly greater than a natural aggregate (NA), but lower than other recycled materials [9].

* Corresponding author.
E-mail address: flora.faleschini@unipd.it (F. Faleschini).

https://doi.org/10.1016/j.conbuildmat.2024.135837
Received 6 November 2023; Received in revised form 17 February 2024; Accepted 12 March 2024
Available online 18 March 2024

In the past, several authors demonstrated that excellent properties can be achieved when EAFS is used to replace the coarse fraction of NA in concrete [10–15]. In this kind of concrete, all mechanical properties are typically improved: this is due to some co-causes, i.e., the higher strength of EAFS particles compared to NAs, the rough surface which promotes a strong bond with the cementitious matrix, and an intrinsic slight hydraulic activity [12–16]. Such beneficial effect depends also on the slag type: indeed, when a more porous slag is employed, the strength development is less evident. However, in average, strength increases by 35–40% when EAFS is used [17]. Conversely, workability is generally worsened, because the peculiar EAFS shape and surface texture strongly affects this property [11]. EAFS concrete displays typically a higher density than NAC, and this also poses the risk for aggregate segregation in the concrete fresh state (slag density is about 30–40% higher than ordinary aggregates, e.g., limestone). Concerning durability properties of EAFS concrete, slag porosity affects strongly freeze/thaw resistance, water penetration, wetting/drying resistance, resulting in worse durability in case of porous slag use. According to Andrade et al. [18] and Sosa et al. [19], EAFS concretes display a better behavior against carbonation. Lastly, Beaucour et al. [20] demonstrated EAFS concrete is more stable to linear expansion and contraction when exposed to high temperatures.

The effectiveness of EAFS concrete use as a structural material was also verified already through tests on real-scale elements, e.g., reinforced concrete (RC) beams under flexure-shear [21–23], RC columns under axial loading [24] and RC beam-column joints under lateral loading [25]. In terms of structural reliability, EAFS concrete showed similar, or even higher performance than NAC, regardless of the type of considered loading, gravity or seismic one [17,26].

When a structural analysis is carried out, characterizing the mechanical performances of the materials is necessary; furthermore, to predict the service life of a structure, durability-related properties should be assessed, too. Understanding the behavior of construction materials under cyclic loading, i.e. alternating loading/unloading steps, is of practical interest for many applications, e.g. for the design of offshore systems, nuclear containments, bridges, and other RC structures that need to withstand seismic loads. Cyclic solicitations may be generated also by wind, waves, traffic other than earthquakes. Repeated loads on structures can be divided into fatigue solicitations, when many cycles of loading of relatively low stress level are applied, and incremental solicitations, which occur under a relatively small number of load cycles of rather high stress. Past works attempted to study and predict the behavior of plain and reinforced concrete under both these solicitations [27–29], but only in the recent years an increasing interest has grown also for other types of sustainable concrete. Among them, recycled aggregate concrete (RAC) with C&DW is undoubtedly the most studied: in [30–32], authors investigated the behavior of RAC under fatigue loading, whereas in [33,34] RAC was subject to cyclic actions. Dealing with the latter problem, Hu et al. [33] demonstrated similar failure modes under monotonic and cyclic loading for both NAC and RAC. However, after failure RAC specimens showed more small and inclined cracks on the surface, while most NAC samples collapsed with only one sub-vertical crack. The same authors highlighted that a partial replacement of NAs with recycled aggregates (RAs) may be more detrimental than a complete replacement. Gonzalez-Fonteboa et al. [34,35] studied the effect of RA on damage of RAC. Results showed that the critical stress, which is the applied stress level that triggers concrete volume expansion rather than continuing to contract [36], decreases with the increase of RA content in the mix. Furthermore, the authors demonstrated that, for any value of the applied stress, damage increases with the replacement ratio of RA. This result is linked to the propagation of cracks at a micro-level. According to many authors [36,37], initially concrete presents microcracks that remain stable up to 30–40% of the compressive strength value; after, they start to propagate within the interface zone. A continuous and rapid crack growth is recorded when concrete under increasing load starts to expand instead than continuing to contract, this transition point represents the minimum volumetric deformation $\varepsilon_{v,min}$ and its corresponding stress value is called critical stress σ_{cr} [36]. Among the other possible recycled materials used as concrete aggregate, the effect of rubber particles to replace NAs was studied by Elghazouli et al. [39]. In comparison with conventional concrete samples, rubberized concrete members exhibit softer cracking behavior leading to favorable ductility and energy dissipation properties. Additionally, increasing the rubber content decreases concrete stiffness, as expected.

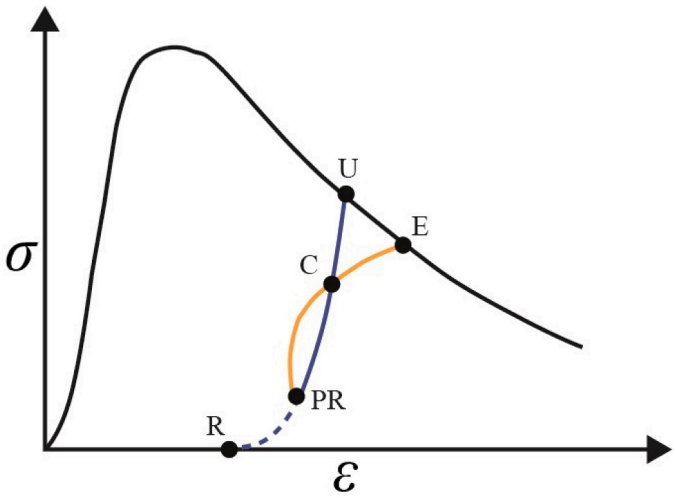

Fig. 1. A hysteresis loop for concrete under cyclic loading and its characteristic points. U: Unloading point; R: Residual point; PR: Partial residual point; C: Common point; E: End point.

Concerning the stress-strain behavior of concrete under cyclic loading, Sinha et al. [40] introduced the concept of uniqueness in the stress-strain relations, which stated that a set of curves can be used to predict the response of plain concrete to any arbitrary axial load history. They demonstrated through both complete and partial unloading that the uniqueness can be reasonably assumed for plain concrete. Performing tests on prismatic specimens subject to cyclic axial load, Shah and Winter [41] reported that a shakedown occurs when approaching a critical load which corresponds to a sharp and continuous microcracks increase. As a further step, Karsan and Jirsa [42] tested rectangular concrete columns under four different loading regimes, and according to the results they proposed a non-uniqueness concept: loading-unloading curves are not unique to a given stress level, but dependent on unloading and reloading response on the previous load history. Bahn and Hsu [43] validated this approach through random cycles results, too. Palermo and Vecchio [44] proposed a model consistent with the compression field approach considering the concrete in both compression and tension, the unloading and reloading curves were linked to the envelope curve obtained by monotonic loading. Sima et al. [45] gave a detailed description of the strength and stiffness decays produced by repeated loads, also proposing a constitutive model for concrete under axial loading, even considering the transition between opening and closing of cracks. Aslani et al. [46,47] proposed compressive and tensile stress-strain models gathering formulas from previous works and introducing independent damage parameters.

The typical hysteresis curve for concrete under cyclic loading comprises unloading and reloading paths, over which it is possible to build the skeleton curve, connecting the peak points of each cycle. Generally, the skeleton curves are similar to the stress-strain curves obtained during a monotonic loading test. Observing a loop of unloading-reloading paths, four characteristic points can be defined: the unloading point (U), the residual point (R) or partial residual point (PR), the common point (C), which represents the intersection between loading and unloading, and the end point (E), where the reloading branch reaches

Table 1
Concrete mix details (kg for 1 m^3).

	NAC1	EAF1	NAC2	EAF2	BAR
Cement dosage	400	400	400	400	400
Cement type	IV/A (V) 42.5 R	IV/A (V) 42.5 R	I 52.5 R	I 52.5 R	I 52.5 R
Water	200	200	160	160	160
w/c	0.5	0.5	0.4	0.4	0.4
NA 0–4 mm	862.5	862.5	913	966	897
NA 4–16 mm	1026.5	-	971	-	-
EAF 4–16 mm	-	1423.5	-	1270	-
BAR 4–14 mm	-	-	-	-	1371
WRA	3.2	4.8	3.2	4.0	4.0

skeleton curve. According to many researchers [42,43], when concrete is loaded and then unloaded to zero stress level, the unloading curve is concave and characterized by high stiffness at the start, whereas the reloading curve is more like the monotonic envelope. Thus, a power-type function is usually preferred to predict the unloading path, while a linear or power-type equation is commonly employed for the reloading branch [33,47]. Fig. 1 shows a typical loop recorded during a cyclic loading test. An example of these observations was obtained by Hu et al. [33] for RAC. There, the skeleton curves almost coincide with those pertaining to the monotonic loadings, similarly than for NACs [42,43]. Hu et al. [33] applied the model proposed by Guo [48] and extended by Xiao el. [49] for modelling the skeleton curves for both NAC and RAC; they have also suggested predictive equations for loading and reloading cyclic loop curves, obtaining excellent agreement with experimental results. Yang et al. [50] confirmed the goodness of this approach in a more recent work, as a proof of the possible extendibility to RAC of previous literature models based on NAC.

According to the best knowledge of the authors, until now there are no published works on EAFS concrete subject to uniaxial cyclic loading. Thus, this work aims to contribute solving this research gap. Experimental results obtained for five concrete mixtures are presented, that differ per the aggregate types and per the curing time. Particularly, we present the results for specimens cured under standard conditions for 28 days (one NAC and one EAFS concrete) and even for cylinder specimens that were cast more than 6 years ago (one NAC, one EAFS concrete and one containing baritic aggregates). These results constitute a significant improvement in the current literature on EAFS concrete, specifically on the long-term properties of this kind of sustainable material. Furthermore, two models are proposed at the end of this manuscript, which can be adopted to describe the full stress-strain behavior of NAC and EAFS concrete under repeated unloading-reloading cycles.

2. Materials and methods

2.1. Materials and mix details

Five concrete mixtures were investigated: NAC1, EAF1, NAC2, EAF2 and BAR. The mixtures can be grouped in two sets, according to the mix details shown in Table 1. The first set aims to investigate the cyclic behavior of concrete in the short term, i.e., after 28 days, other than the main mechanical properties. This group of concretes is made by a conventional (NAC1) and an EAFS mix (EAF1), and there a cement type CEM IV/A (V) 42.5 R was used, according to EN 197–1 [51], with w/c ratio = 0.5. This binder, currently very used in the Italian market context, contains about 30% of fly ash (FA) replacing clinker, allowing to limit the environmental footprint compared to the concretes belonging to the second group. The second set aims instead to investigate the cyclic behavior of concrete in the long term, i.e., after six years from casting, other than the main mechanical properties, which were evaluated at 28 days. This group is made again by a conventional (NAC2), an EAFS concrete (EAF2), and additionally one with baritic aggregates (BAR). The mixes were prepared using a Portland cement CEM I 52.5 R, according to EN 197–1 [51] with a reduced water dosage, resulting in a w/c ratio equal to 0.4. At the age of these concretes casting, CEM IV/A (V) 42.5 R was instead not very common, and for laboratory practices, Portland cement was very often adopted as done in the present case. The choice of investigating baritic concrete was due to producing a heavyweight concrete with similar density to that made with EAFS. This comparison is particularly interesting considering the applications of heavyweight concrete as shielding against radiation in the eventuality of exposing them to cyclic loading, as in nuclear plants. In fact, Pomaro et al. [52] demonstrated that the shielding properties of EAFS concretes are similar or even higher than those measured for baritic concrete.

Table 2
Physical properties of the aggregates.

	NA 0–4	NA 4–16	EAF 4–16	BAR 4–14
S.S.D. Density (kg/m^3)	2644	2769	3808	3817
Water Absorption (%)	2.71	1.37	0.91	1.90
Shape	Round	Round	Sharp-pointed	Sharp-pointed

In both sets, the EAFS concrete include slag at 100% of the coarse fraction of aggregates, whereas the fine fraction was maintained the same as that in the NAC (with natural sand). All the concretes analyzed here contain a sulphonated naphthalene water reducing admixture (WRA), to reach an adequate workability. Generally, slag concrete requires a higher dosage of WRA since the use of EAFS decreases workability, as stated in previous works [53]. For all mixtures, tap water from the water supply of Padova city was used, that does not contain any harmful substance.

Table 2 shows the physical properties of the aggregates, among them, S.S.D. density and water absorption were measured according to EN 1097–6 [54]. It is worth noting that barite and EAFS have similar shape, surface texture and density (Fig. 2). In Fig. 3, the grading curves of the aggregates employed in this experimental investigation are shown.

After concrete mixing and casting, all the samples were covered with plastic bags, and after 24 hours they were removed from molds and cured in water at 20±1°C for 28 days. As stated, two times of testing were chosen: 28 days (standard curing time) and a prolonged time, here selected as six years. The specimens that underwent this prolonged maturation were placed in a protected environment in the laboratory, approximately at RH = 50% and T = 20°C. The curing chamber consists of an insulated room where an air conditioning system maintains a constant relative humidity and temperature. The two curing times were chosen aimed at characterizing both the short- and long-term behavior of EAFS concrete under cyclic uniaxial compression: the first set allows us to compare cyclic and monotonic compression behavior at 28 days, while the second set is a useful extension of the results in long-term. However, as recalled already in Section 2.1, two different mix details were used (to reflect the new trend of the Italian market in terms of adoption of cement type, the last mix was made with a pozzolanic cement in place of Portland one, which use is dropped significantly close to null except for specific laboratory tests), thus a direct comparison between results of the two mixes is not possible.

2.2. Test methods and setup

For each mixture, a series of cylinders with dimensions d x h = 100 ×200 mm were cast to evaluate the compressive strength (f_c), the indirect tensile strength (f_{ct}) and the overall cyclic compressive behavior.

Compressive (f_c) and tensile strength (f_{ct}) were tested according to EN 12390-3 [55] and EN 12390-6 [56], respectively, under force control at a speed rate of 0.5 MPa/s and 0.05 MPa/s, respectively. Concerning the cyclic loading protocol, there are no specific standards that we can refer to, hence the adopted setup is based on [55] with some differences. First, samples were equipped with four strain gauges (SGs): two were

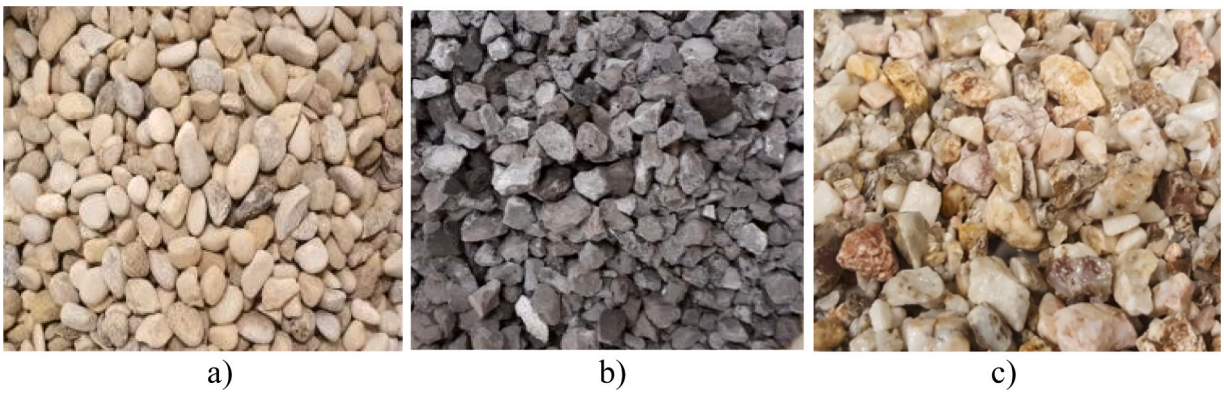

Fig. 2. Aggregates employed in this work: a) NA 4-16, b) EAFS 4-16 and c) barite 4-14.

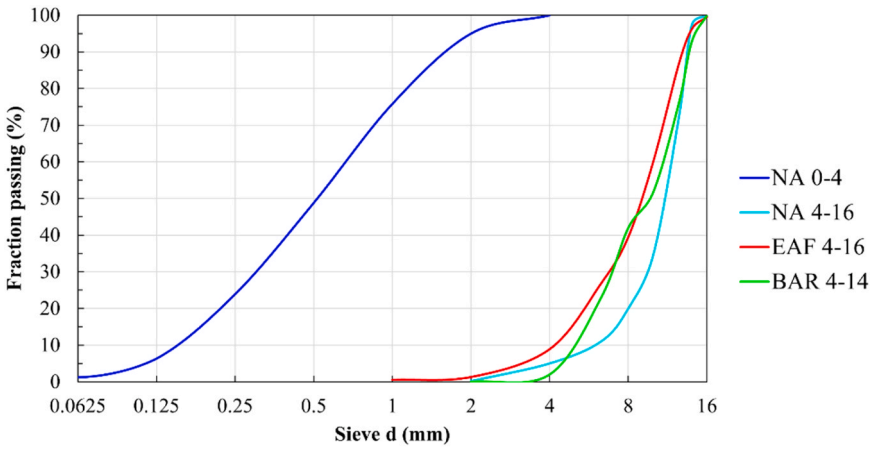

Fig. 3. Grading curves of the aggregates employed in this work.

placed transversally, and the others longitudinally (see Fig. 4 for their location onto the lateral surface of the specimens). Fig. 5 shows instead the applied loading history: it consists of several alternated cycles of loading and unloading. The first part was performed under a force-control mode, at a speed of about 0.1 MPa/s. After a brief stabilization phase, three stress levels were applied, being 0.1, 0.3 and 0.5 f_c, with two loading cycles per applied stress level. In the second part, the load was increased under a displacement-control mode, that was 0.3 mm/min, with single loading cycles, that consist in steps of +0.3 mm. Between each loading and unloading cycles, and vice versa, there was a 10 second stabilization phase. The load application stopped after reaching the peak load as no post-peak branch was visible for any sample.

As stated, two times of testing were chosen for the cyclic compressive strength: 28 days strength (f_{cc}) and a prolonged time, here selected as six years strength ($f_{cc,6y}$). Table 3 shows the test matrix of this experimental campaign, i.e., the number and type of tests performed per each mixture.

3. Experimental results

3.1. Mechanical characterization

Table 4 lists the fresh and hardened concrete properties, in terms of: Abram's cone slump according to EN 12350–2 [57], fresh density (ρ_{fc}), hardened density (ρ_c) at 28 days of curing, compressive strength (f_c) and tensile strength (f_{ct}) at 28 days of curing.

The workability of the mixture was slightly reduced when containing EAFS, this is due to the well-known shape effect of EAFS [11], but it is worth noting barite is responsible for a similar effect. To solve this issue, a higher dosage of WRA was employed in concretes with slags. According to [58], NAC1, EAF1 and BAR fall into S3 consistency class (100 – 150 mm slump range), while the others are classified as S4 (160 – 210 mm). Both hardened and fresh density are increased in EAFS and BAR concretes than in NACs, due to the higher particle density of the aggregates: the increase is about +15% for EAFS concrete, and + 20% for the baritic one. There are no significant differences between the fresh and the hardened densities for each concrete batch: this is the result of a curing performed minimizing water evaporation, i.e., covering the fresh concrete with water-proof bags and soaking the samples in water until 28 days, which allows a better hydration and a minimal weight variation.

Concerning the mechanical properties, experimental results confirm the positive effect of replacing NAs with EAFS. Regarding the first set of mixtures, compressive and tensile strength are improved by +37% and +28%, respectively, compared to NAC. The same trend is confirmed by the second set of mixtures: EAF2 compressive strength is +41% and +46% higher than conventional and baritic concrete. These results are due to several beneficial effects of the slag, i.e., the good adhesion between the slag and the matrix [12], the intrinsic higher strength of EAFS compared to other aggregates [12], the high quality of interfacial transition zone (ITZ) [16]. It is worth noting that the replacement of NAs with barite is not convenient from a sole mechanical point of view, because the increase of density is not counterbalanced by an enhancement of the strength.

Comparing the two sets of mixtures and recalling that they are made adopting two different cement types, different proportions of their constituents, among which a different w/c ratio, it is possible to observe that concretes made with CEM IV/A 42.5 R type exhibited similar

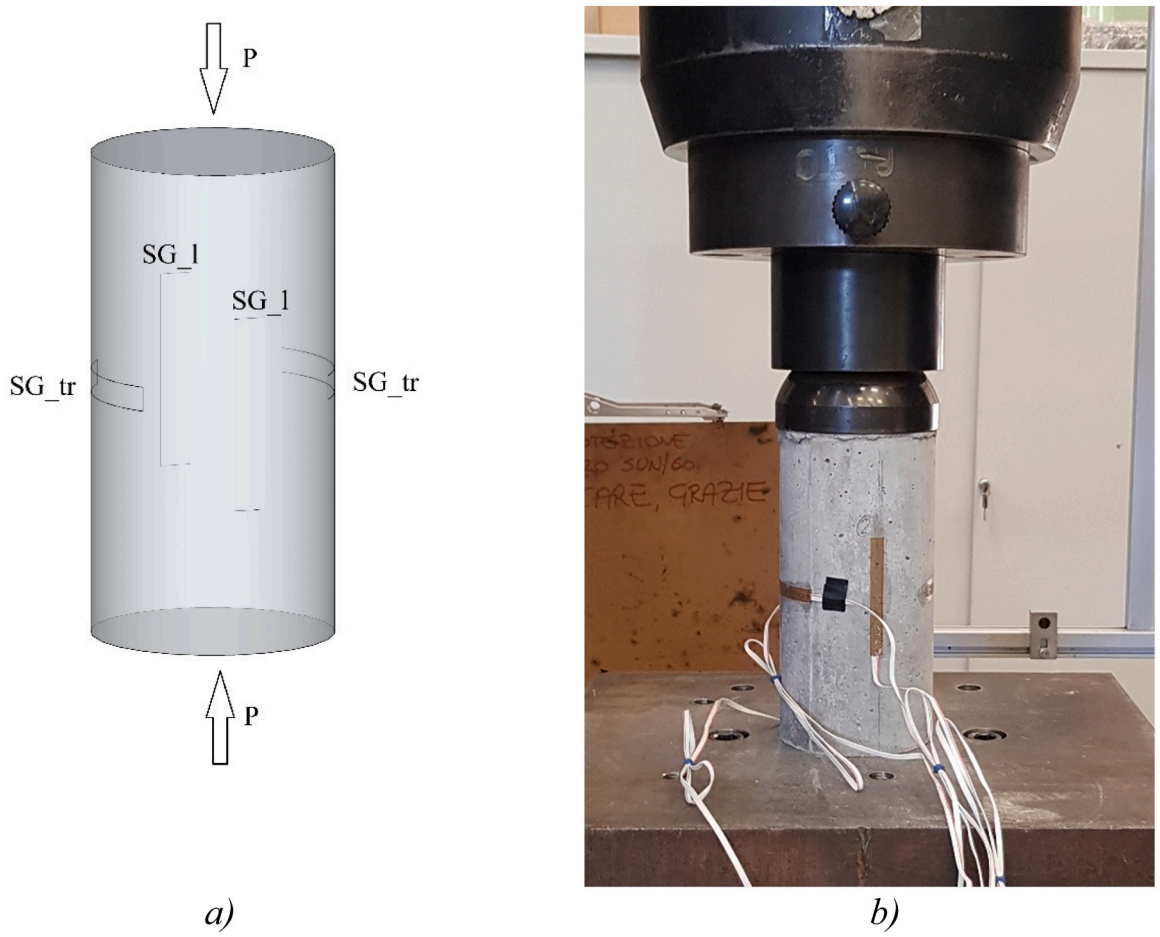

Fig. 4. Test setup of the cyclic compression test: a) scheme; b) photo. SG_l: Longitudinally-placed strain gauge; SG_tr: Transversally-placed strain gauge.

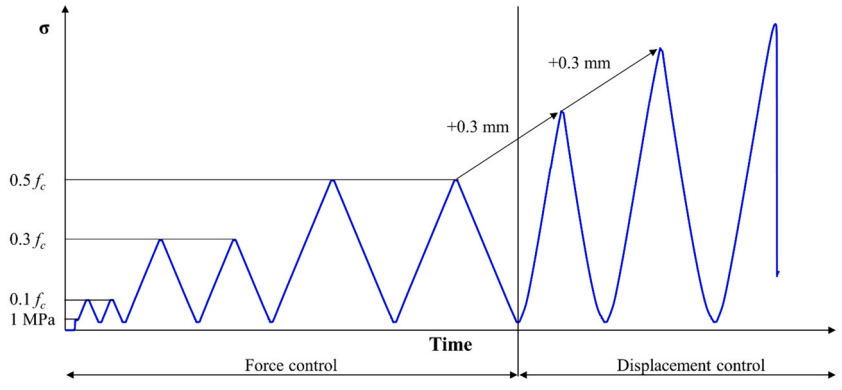

Fig. 5. Loading history of the cyclic test.

Table 3
Test matrix for this experimental campaign.

Test		NAC1	EAF1	NAC2	EAF2	BAR
Fresh density	ρ_{fc}	3	3	3	3	3
Hardened density – 28d	ρ_c	3	3	3	3	3
Compressive strength – 28d	f_c	3	3	3	3	3
Splitting strength – 28d	f_{ct}	3	3	3	3	3
Cyclic compressive strength – 28d	f_{cc}	2	2	-	-	-
Cyclic compressive strength – 6 y	$f_{cc,6y}$	-	-	2	2	2

Table 4
Average fresh and hardened concrete properties.

		NAC1	EAF1	NAC2	EAF2	BAR
Slump (cm)		12.0	10.0	19.0	21.0	15.0
ρ_{fc}	μ (kg/m^3)	2407	2824	2390	2817	2884
	COV (%)	0.46	0.39	0.35	0.54	1.30
ρ_c	μ (kg/m^3)	2431	2828	2404	2830	2828
	COV (%)	0.43	0.11	0.24	1.18	0.85
f_c (MPa)	μ (MPa)	38.96	53.34	41.24	58.00	39.70
	COV (%)	1.64	0.84	0.44	3.05	1.94
f_{ct} (MPa)	μ (MPa)	3.56	4.56	3.32	4.24	3.36
	COV (%)	9.83	6.80	14.97	4.67	6.61

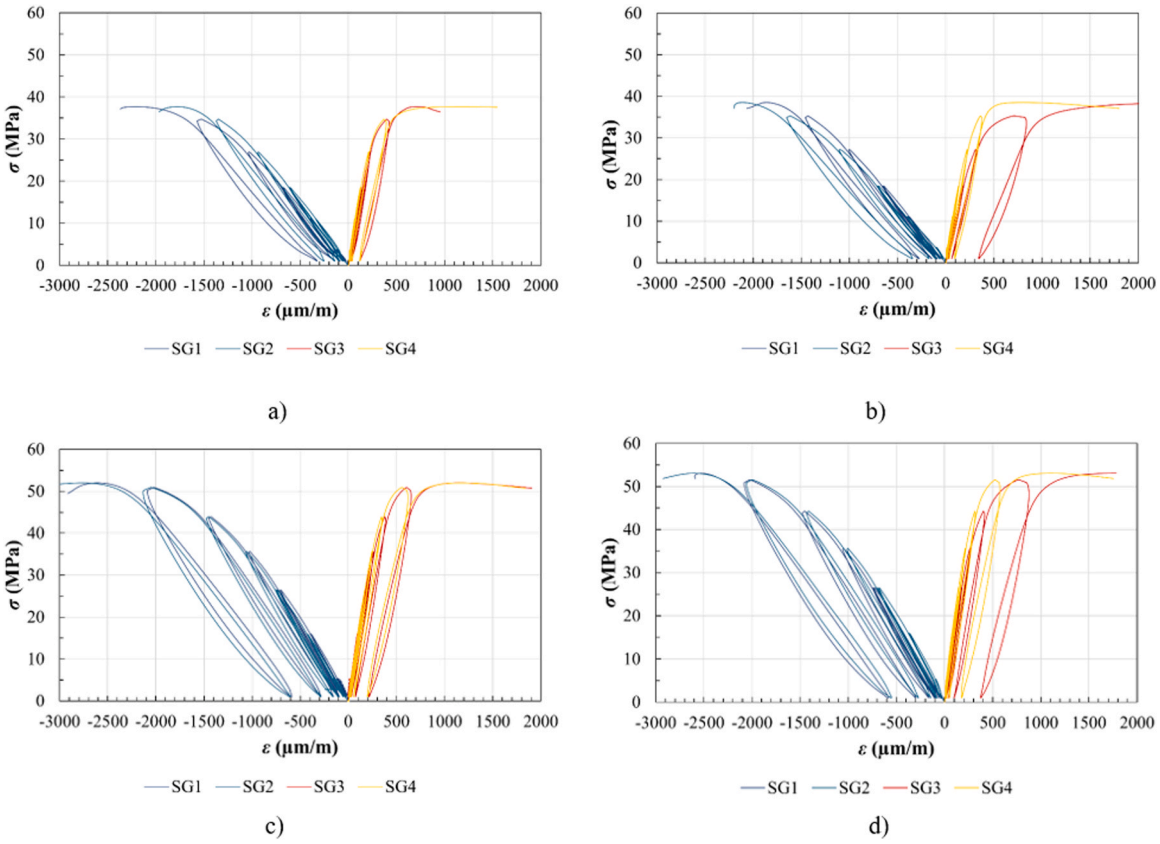

Fig. 6. Results of short-term cyclic compression tests: a) NAC1_1; b) NAC1_2; c) EAF1_1; d) EAF1_2. SG1 and SG2 stand for longitudinal SGs, SG3 and SG4 stand for transversal SGs.

strength than those made with CEM I 52.5 R. Such a result is particularly interesting if compared to the unsuccessful results obtained by other researchers in attempting to use alternative cement types other than Portland one (i.e., CEM IV/B). The interaction between slag and pozzolanic cement is thus a matter to be analyzed in further studies.

Another interesting aspect resulting from comparing the two sets is the relationship between splitting strength and compressive strength. In this case, the second series has a comparatively low tensile strength despite its higher compressive strength than that of the first series. However, it should be recalled that splitting strength has a relationship with compressive strength, but it is not linear [59]. Generally, as compressive strength increases, the tensile strength increases as well, but at a lower rate. The tensile strength depends also on w/c ratio, cement type and temperature of curing, and these parameters may have a different influence than for other mechanical properties [59]. Specifically, cement type, and more generally speaking the cementitious matrix (cement, filler, SCMs, etc) plays an important role. When clinker is replaced by pozzolanic materials, e.g. fly ash or silica fume, up to 10% of its mass, tensile strength increases at a higher rate than compressive strength [60]. The beneficial effect of adding such SCMs is evident for both compressive and splitting strength, but the percentage increase is more important for the indirect tensile strength [60]. The first series was cast with a pozzolanic cement containing fly ash, whereas for the second one a Portland cement was employed: this can explain the comparatively lower tensile strength of the second series despite its higher compressive strength. Apart from these aspects, the results of the splitting strength test of the second series are more scattered, and this is a further aspect that should be considered.

Table 5
Results of cyclic loading tests on the first set of specimens.

	f_{cc} (MPa)	$\varepsilon_{l,u}$ (μm/m)	$\varepsilon_{tr,u}$ (μm/m)	$\varepsilon_{v,min}$ (μm/m)	σ_{crit} (MPa)	σ_{crit}/f_{cc} (-)
NAC1_1	37.69	-2000	967	-672	33.90	0.899
NAC1_2	38.55	-1984	1724	-572	32.18	0.835
Ave. NAC1	38.12	-1992	1345	-622	33.04	0.867
EAF1_1	52.01	-2676	1150	-877	50.93	0.979
EAF1_2	53.04	-2565	1444	-778	48.46	0.914
Ave. EAF1	52.53	-2620	1297	-828	49.70	0.947

3.2. Cyclic loading behavior

3.2.1. First set of concretes: short-term cyclic tests

Fig. 6 shows the full stress-strain curves of the concretes belonging to the first set (from here, short-term cyclic tests), performed at 28 days of curing. Strain gauges record positive values for extension and negative values for contraction, hence the transversally oriented SGs reported strain values in the right part of the graph; oppositely, longitudinal SGs are graphed on the left part.

Table 5 lists the cyclic compressive strength (f_{cc}), the ultimate longitudinal strain ($\varepsilon_{l,u}$) and ultimate transverse strain ($\varepsilon_{tr,u}$) recorded during the short-term cyclic tests. First, it is worth noting that the cyclic compressive strength f_{cc} is quite similar to that tested under monotonic loading f_c, therefore the loading history does not affect this parameter, as expected [33,45]. Concerning the failure mode, all specimens failed in a brittle way just after the exceedance of the peak load. In average, EAFS specimens reached a higher peak longitudinal strain and a lower transverse peak strain than NAC, being about +31% and −4%,

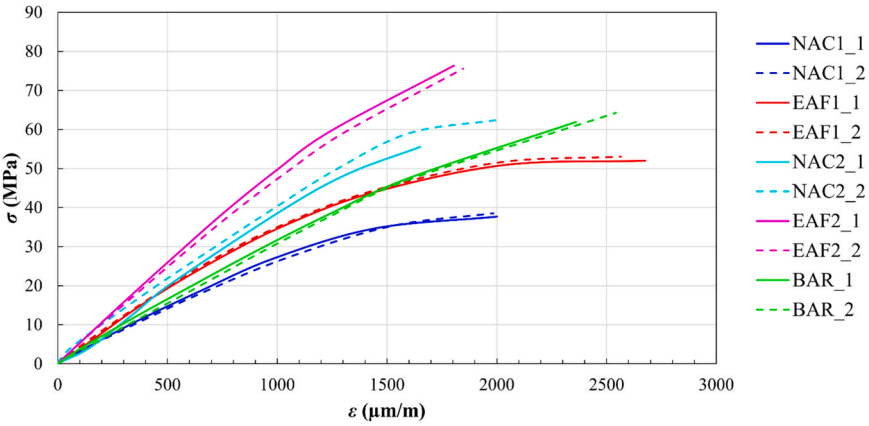

Fig. 7. Skeleton curves for cyclic compression tests.

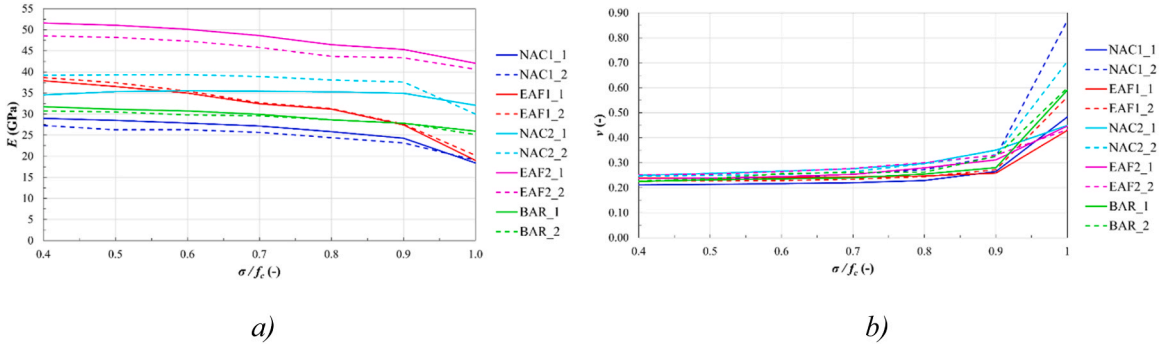

Fig. 8. Deformative properties of tested specimens under cyclic compression: a) Secant Modulus; b) Poisson's coefficient.

respectively.

From the cyclic curves it is possible to draw the skeleton curves (Fig. 7), obtained connecting the peak points of each applied loop, considering the average longitudinal strain recorded by the two SGs; these curves are similar to those recorded for a monotonic loading [33]. If one compares these graphs for each concrete type, it will be possible to observe that EAF1 concrete is characterized by an initial slope slightly steeper than NAC1; approaching the peak stress, they become similar. In fact, according to [33,38,61], the analytical calculation of the secant modulus E at different stress levels can be carried out on skeleton curves applying Eq. (1):

$$E = \frac{\sigma_2 - \sigma_1}{\varepsilon_{l2} - 0.005\%} \tag{1}$$

where σ_1 is the stress corresponding to a longitudinal strain of 0.005%, while σ_2 is the stress level related to the ε_{l2} longitudinal strain. Thus, a graphic representation of the secant modulus E calculated at different stress levels is reported in Fig. 8a. Looking at the results for the short-term cyclic tests, E is quite higher in EAF1 concrete at low stress levels: at 0.4 f_c, E is equal to 38.289 GPa in average, against 28.142 GPa for NAC1. At peak load, E is almost the same for both the mixes: the difference is 877 MPa, only. This result demonstrates the utility of a complete characterization of the whole stress-strain curve.

Concerning the transverse behavior of concrete, the Poisson's coefficient ν is usually calculated at 0.4 f_c according to Eurocode 2 (EC2) [62]. Thus, Eq. (2) is hereafter applied for the calculation of ν [38,62]:

$$\nu = \frac{\varepsilon_{tr2} - \varepsilon_{tr1}}{\varepsilon_{l2} - 0.005\%} \tag{2}$$

where ε_{tr2} is the transverse strain and ε_{l2} is the longitudinal strain at the analyzed stress level, whereas ε_{tr1} is the transverse strain corresponding to a longitudinal strain of 0.005%. Similar to the secant modulus E, the Poisson's coefficient is hereafter calculated at different stress levels for a better understanding of the deformative behavior. At low stress levels, i.e. at 0.4 f_c, ν is higher in EAF1 concrete for only 6% in average, compared to NAC1 (Fig. 8b), however it assumes a value in the range 0.20–0.30 for all the tested specimens until 0.8 f_c. After this value, NAC1 is characterized by the highest deformation in the transverse direction: at the peak load, indeed, the mean value of ν, calculated as the average of the peak ν obtained for each test, is 0.676 and 0.496 for NAC1 and EAF1, respectively. Recall however that the values of ν are widely scattered, and there is a loss of significance of the results at the highest stress levels, i.e. between 0.8 fc and fc.

Fig. 9 shows the evolution of longitudinal, transverse, and volumetric strains for each specimen tested with the cyclic protocol, vs. the dimensionless stress (σ / f_{cc}). The average strains between the recorded ones by the SGs are plotted for NAC1_1, NAC1_2, EAF1_1 and EAF1_2. In addition, the skeleton curves are graphed connecting the peak points of each pertaining curve. The volumetric strain ε_v is calculated according to Eq. (3):

$$\varepsilon_v = \varepsilon_l + 2{\cdot}\varepsilon_{tr} \tag{3}$$

A summarized graphical representation of the skeleton curves in terms of longitudinal ε_l, transverse ε_{tr}, and volumetric ε_v mean strains is shown in Fig. 10a. In this graph, the minimum peak volumetric strains were detected, the coordinates of these points in terms of $\varepsilon_{v,min}$, σ_{crit}, σ_{crit}/f_{cc} are shown in Table 5. It is worth recalling that the critical stress σ_{crit} corresponds to the formation of a rapid and continuous cracks pattern when the volumetric deformation ε_v reaches its minimum value [36,38].

EAF1 concrete attains higher values of $\varepsilon_{v,min}$ and σ_{crit}. Microscopically, the critical stress appears to be related to the strength of concrete and to its fracture toughness. However, these are not the unique reasons

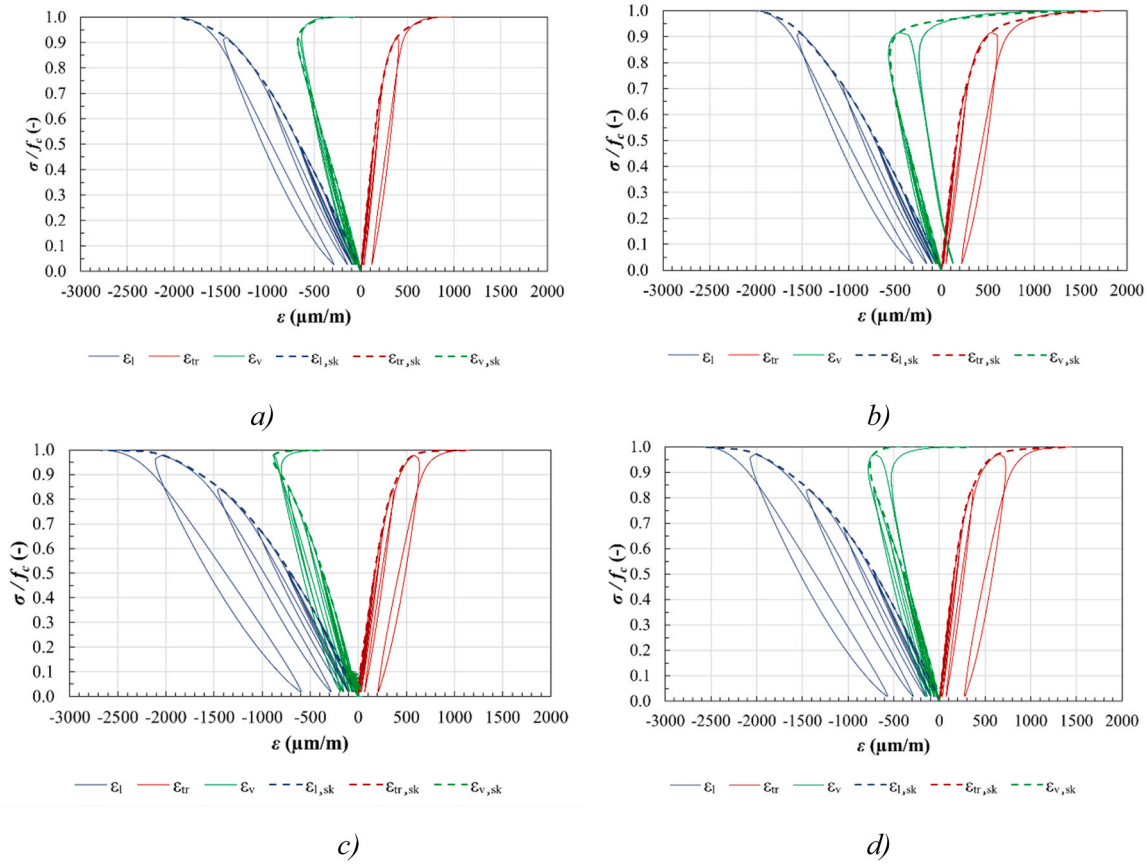

Fig. 9. Results of short-term cyclic compression tests in terms of longitudinal, transverse, and volumetric mean strain: a) NAC1_1; b) NAC1_2; c) EAF1_1; d) EAF1_2. The subscript "sk" refers to the skeleton curve.

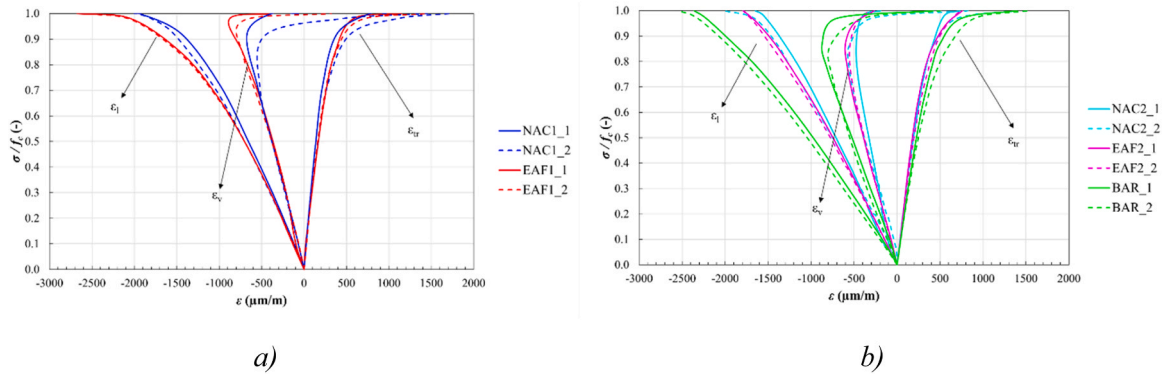

Fig. 10. Skeleton curves of longitudinal, transverse, and volumetric mean strain for cyclic tests: a) first set; b) second set.

responsible for this result: in fact, also the σ_{crit}/f_{cc} ratio is higher in EAFS mixes than in NAC. We suggest that the value assumed by the critical stress can be related to the time of initial crack propagation in concrete, too: recall that EAFS concrete has a stronger ITZ than NAC, and most cracks in compression spread properly from this region. The (relatively) low speed of propagation, and the delayed time of cracking in EAFS concrete may be properly due to the improved bond of cement-aggregates, thanks to the rough surface of the slag [12], but also to the enrichment in the ITZ of the products from the late hydration of the slag itself [16]. Instead, the post-critical stress reservoir is higher in NAC1 than in EAFS concrete: limited differences between the critical and the peak stress value in EAFS concrete confirms its highly brittle behavior, typically observed in high-strength concretes.

Under increasing loading, the material structure faces a progressive deterioration. This phenomenon can be characterized using the variation of E, usually denoted as damage [63]. For a generic material, the dimensionless damage is often quantified according to Eq. (4):

$$D_E = 1 - \frac{E_d}{E_{ini}} \tag{4}$$

where E_d is the secant modulus of the damaged material at a considered stress level, while E_{ini} is the initial E considered as a reference. The skeleton curves at Fig. 7 show an almost constant slope until 0.4 f_c, hence the hypothesis of E_{ini} equal to E at 0.4 f_c of stress is considered reliable for the following calculation of damage. As a support to this consideration, Sima et al. [45] observed that the compression curve of concrete shows a linear response until approximately a half of the compressive strength. The evolution of the dimensionless damage

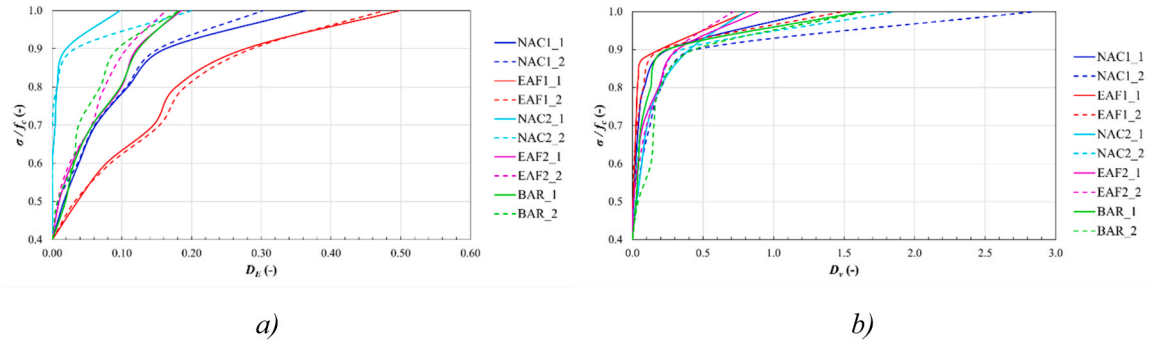

a) b)

Fig. 11. Evolution of damage: a) D_E; b) D_ν.

Table 6
Long-term results for the second set.

	$f_{cc,6y}$ (MPa)	$\varepsilon_{l,u}$ (μm/m)	$\varepsilon_{tr,u}$ (μm/m)	$\varepsilon_{v,min}$ (μm/m)	σ_{crit} (MPa)	σ_{crit}/ $f_{cc,6y}$ (-)	f_c (MPa)	Δ (%)
NAC2_1	55.51	-1437	732	-476	46.55	0.839		
NAC2_2	62.53	-1761	1418	-570	52.53	0.840		
Ave. NAC2	59.02	-1599	1075	-523	49.54	0.840	41.24	43%
EAF2_1	76.40	-1892	1029	-590	64.08	0.839		
EAF2_2	75.61	-1847	798	-557	63.93	0.850		
Ave. EAF2	76.00	-1870	914	-574	64.01	0.845	58.00	31%
BAR_1	61.90	-2360	1394	-879	52.99	0.856		
BAR_2	64.29	-2542	1525	-791	52.89	0.823		
Ave. BAR	63.10	-2451	1460	-835	52.94	0.825	39.70	59%

calculated according to Eq. (4) is reported in Fig. 11a. Considering only the short-term results, the damage evolution is quite similar among the specimens of the same mixture. EAFS concrete displays the most relevant damage growth; in fact, as already stated, E is almost the same for NAC1 and EAF1 concrete at the peak, but is significantly different at low stress levels. Between 0.7 f_c and 0.9 f_c, an inflection of the curves is clearly visible, probably linked to the repeated loading cycle, suggesting a damage evolution which differs from that usually recorded under monotonic axial loading. Indeed, in this last case, the curves are usually smooth without visible inflections [34].

Another approach for quantifying the damage evolution involves the Poisson's coefficient ν. In this case, the damage is calculated according to Eq. (5):

$$D_\nu = \frac{\nu_d}{\nu_{ini}} - 1 \tag{5}$$

where ν_d is the Poisson's coefficient ν of the damaged material at a considered stress level, while ν_{ini} is the initial ν considered at 0.4 f_c. The evolution of damage according to Eq. (5) is presented in Fig. 11b. Focusing on short-term results, the conventional concrete shows a higher mean damage even at medium-low stress level, demonstrating higher tendency to develop transverse deformations. Damage calculated with this approach shows a steep increase after 0.9 f_c because of strong transverse deformations near the peak load.

3.2.2. Second set of concretes: long-term cyclic tests and comparison

In this section, the results of the cyclic tests on specimens cured for more than 6 years are presented, aiming to extend the observation of the previous sections on different samples, characterized however by similar mechanical strength at 28 days. Table 6 summarizes the results showing the values of the cyclic compressive strength at 6 years of curing ($f_{cc,6y}$) and the corresponding $\varepsilon_{l,u}$ and $\varepsilon_{tr,u}$, while Fig. 10b shows the evolution of longitudinal, transverse and volumetric mean strain calculated as explained in the previous section.

In all tests, EAFS concrete demonstrated the highest cyclic strength: $f_{cc,6y}$ is +29% and +20% higher than in NAC and BAR mixes, respectively. As in high-strength concretes, EAF2 approached the peak load with limited traverse deformations occurrence, while NAC2 showed the lowest longitudinal ultimate strain. As observed in the previous sections and by other authors [33], compressive strength under monotonic and cyclic loading is generally similar, and for this reason, results are clearly understandable due to the strength difference among NAC2, BAR and EAF2. Table 6 shows the strength gain Δ over time for the second set of mixes, moving from 28 days (f_c) to 6 years $f_{cc,6y}$ of curing. Baritic concrete showed the highest strength gain, i.e., 59%. Conversely, EAFS concrete reported a strength gain of only 31%, which corresponds to 18 MPa. This result, i.e., a less strength gain of EAFS concrete in the prolonged time compared to other concrete types, was already observed by Rondi et al. [64], who showed that a concrete with 100% EAFS replacing conventional aggregates reached its maximum strength capacity after 120 days of curing, with almost negligible strength increase at higher ages.

In Fig. 8a, a complete comparison of E evolution for all the tested specimens is shown. Particularly, within the second set, EAF2 and BAR demonstrated the highest and the lowest values of Young Modulus, respectively; the difference remains remarkable also at the peak load, differently from the trials of the first set. It is worth recalling that baritic concrete is generally characterized by low deformative properties, due to the specific mineralogy of the barite itself, which is made of relatively soft barium sulphate particles. These minerals may also contain smeared cracks, which are filled by powdery material made of barite, iron oxide and clay [65]. The mixtures of the second group NAC2 and EAF2 are stiffer than NAC1 and EAF1, and this result is directly linked to the higher compressive strength of these specimens. Furthermore, NAC2, EAF2 and BAR showed a less pronounced E reduction, at increasing stress levels: on average, E decreases by about −16%, −17% and −18% moving from 0.4 f_c to f_c, for NAC2, EAF2 and BAR, respectively. This reduction was about −33% and −51% in NAC1 and EAF1.

The same comparison in terms of Poisson's coefficient is shown in Fig. 8b. All ν values are within the range 0.20–0.30 until 0.8 f_c: beyond this threshold, the scattering of data becomes more significant; leading to a not meaningful comparison from 0.8 f_c to f_c. However, until 0.8 f_c, the specimens of the second set NAC2 and EAF2 showed higher values of ν in average.

Fig. 10b shows the evolution of longitudinal, transverse and volumetric mean strain (calculated as explained in the previous section); furthermore the coordinates of the minimum peak points of volumetric strain are shown in Table 6 in terms of $\varepsilon_{v,min}$, σ_{crit}, σ_{crit}/f_{cc}. In this case, most of the results already obtained for the short-term cyclic compression can be extended, with few differences. EAFS concrete has higher σ_{crit} and σ_{crit}/f_{cc} than other counterparts, but the difference in this case is less pronounced. Indeed, the normalized σ_{crit}/f_{cc} of EAF2 is higher by just 0.005 and 0.020 than NAC2 and BAR, respectively. This result confirms that EAFS concrete achieves more rapid strength gains in the short term. In the second set of cyclic tests, BAR attained the highest absolute volumetric expansion, confirming its soft and deformable behavior. Comparing NAC2 and EAF2, the same trend already observed for the first set of tests is confirmed: EAF2 reached higher $\varepsilon_{v,min}$ than those of NAC2. In average, the post-critical reservoir is higher in the specimens of the second set: probably, this difference is due to the different age of curing of the samples. Gonzalez-Fonteboa et al. [34] found σ_{crit}/f_c values higher than 0.90 for specimens tested at 28 days made with limestone aggregates, but such σ_{crit}/f_c ratio decreases with the increase in the percentage of recycled coarse aggregate. Therefore, the aggregate type can effectively modify the σ_{crit}/f_{cc} ratio: the higher hardness of the aggregates, the higher critical stress can be reached. This work confirms such observation because EAFS, which is typically hard and sound, provides the highest values of σ_{crit}/f_{cc} when it is employed in concrete production. Another aspect concerns the age of curing, indeed both the results from Gonzalez-Fonteboa et al. [34] and those of this work (first set) show average σ_{crit}/f_{cc} values higher than 0.85 at 28 days of curing, while the same parameter is lower than 0.85 for the second set at 6 years of curing. As a result, longer curing time may provide lower σ_{crit}/f_{cc}, but this observation needs to be confirmed by other experimental evidence.

The evolution of damage is carried out similarly than before, and results are shown in Fig. 11. Damage evolution D_E is quite similar between BAR and EAF2, conversely NAC2 remains almost undamaged until $0.9\,f_c$. In the long-term tests, damage evolution seems to be less pronounced than in specimens tested in the short-term. The curves in Fig. 11a present several inflections, demonstrating a non-uniform increase of damage. Also in this case, it is possible to attribute a different damage evolution due to the cyclic loading protocol, compared to what observed for instance by Gonzalez-Fonteboa et al. [34] under monotonic tests, where uniform damage occurred.

Damage evolution D_ν for the second set of concretes is calculated as for the first one according to Eq. (5), and results are shown in Fig. 11b. In average, the second set confirms higher values of D_ν for NAC2 and BAR, particularly when approaching the peak load. As for the damage D_E, the curves graphed in Fig. 11b have some inflection points, and this trend can be attributed to the cyclic loading protocol. Near the peak, EAF1 and NAC1 show higher mean D_ν than the corresponding mixtures of the second set.

4. Discussion

In this section, the assessment of the accuracy of models to predict the main parameters of the constitutive equations of NAC and EAFS concrete is carried out (Section 4.1). Further, analytical stress-strain models to predict the cyclic compression behavior of EAFS concrete are proposed (Section 4.2).

4.1. Elastic modulus: comparison with EC2 and ACI code formulations

A comparison between experimental results and theoretical provision models is carried out. According to EC2 [62], the average Young Modulus E_{cm} can be determined according to Eq. (6):

$$E_{cm}(MPa) = 22,000\left(\frac{f_{cm}}{10}\right)^{0.3} \tag{6}$$

Table 7
Comparison of Elastic Modulus between experimental value and theoretical predictions.

	NAC1	EAF1	NAC2	EAF2	BAR
$E_{cm,\ exp}$ (MPa)	28142	38289	36876	50056	31238
$E_{cm,\ EC2}$ (MPa)	29774	43624	33726	48512	38232
Variation EC2 (%)	-5.80	-13.93	8.54	3.08	-22.39
$E_{cm,\ ACI1}$ (MPa)	31509	46836	38365	55710	52584
Variation ACI1 (%)	-11.96	-22.36	-4.04	-11.29	-68.33
$E_{cm,\ ACI2}$ (MPa)	29541	34568	36361	41261	37597
Variation ACI2 (%)	-4.97	9.72	1.40	17.57	-20.36

where f_{cm} is the average compressive strength at 28 days of curing. As recalled in EC2 [62]: "For limestone and sandstone aggregates the value should be reduced by 10% and 30% respectively; for basalt aggregates the value should be increased by 20%". The NAs employed in this research are a mix of siliceous and sandstone aggregates, therefore a −10% reduction can be considered reliable in this case for NAC. Instead, a correction factor equal to +20% is applied for EAFS concrete as steel slag and basalt aggregates have similar physical properties.

ACI code [66] proposes instead two relationships according to Eqs. (7) and (8). These models are hereafter called ACI1 and ACI2, respectively:

$$E_{cm}(MPa) = w_c^{1.5}0.043\sqrt{f_c} \tag{7}$$

$$E_{cm}(MPa) = 4700\sqrt{f_c} \tag{8}$$

where w_c is the average bulk density (in kg/m^3), f_c is the compressive strength of concrete at 28 days (in MPa). Eq. (7) is proposed for w_c values between 1440 and 2560 kg/m^3, while Eq. (8) is intended for normal-weight concrete. No formulations are available for heavy-weight concretes or to consider alternative aggregate types.

Table 7 shows a comparison between experimental and theoretical E_{cm} values obtained according to Eqs. (6), (7) and (8). EC2 [62] model was employed applying a −10% and +20% correction for NAC and EAFS, respectively, according to the previous considerations. The experimental values of E_{cm} are considered as secant Modulus at $0.4\,f_c$ calculated according to Eq. (1), the variation is instead evaluated according to Eq. (9):

$$Variation(\%) = \frac{\left(E_{cm,\exp} - E_{cm,code}\right)}{E_{cm,\exp}} \times 100 \tag{9}$$

Most models overestimate the experimental values; however, EC2 and ACI2 formulations provide most accurate predictions. Results of ACI1 are quite far from the real values, but it is worth mentioning that EAFS and BAR concrete density are out from the range for application of this formulation. The Elastic Modulus for BAR is not well-predicted by any code, as barite consists of highly dense but deformable gravel particles, which are totally different from other aggregates for which these formulas are calibrated.

Considering the overall variations for all conglomerates, EC2 and ACI2 seem to provide the most affordable values, but proper corrections factors should be employed according to the aggregates type.

4.2. Analytical stress-strain models for EAFS under cyclic loading

4.2.1. Constitutive relations under cyclic loading

In this section an analytical model for predicting the stress-strain (σ - ε) relation under cyclic loading of a concrete containing EAFS is proposed. Many works in literature have attempted to propose constitutive relations for cement-based materials under cyclic or fatigue loading, even when including slags [67,68], but never for EAFS concrete. The approach presented here is similar to that employed by Hu et al. [33] for RAC containing aggregates from C&DW.

From now, x and y are defined as the dimensionless strain and stress,

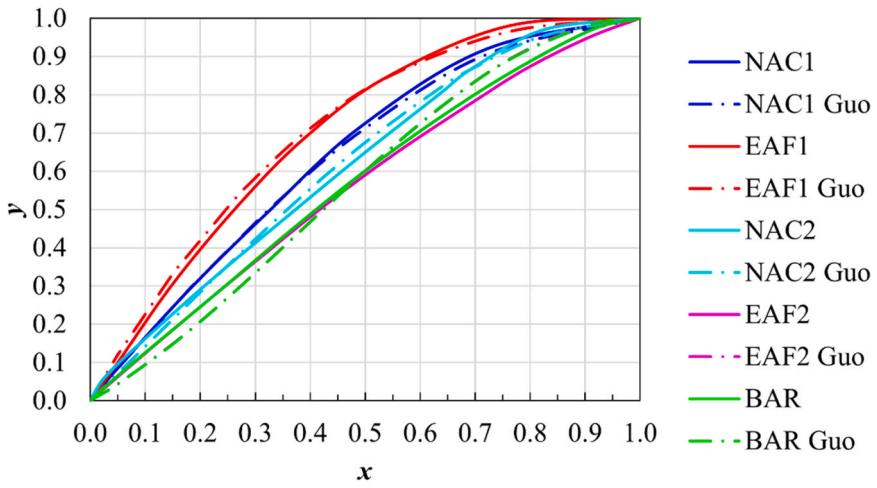

Fig. 12. Experimental vs. calculated skeleton curves.

respectively according to Eqs. (10, 11):

$$x = \frac{\varepsilon}{\varepsilon_u} \tag{10}$$

$$y = \frac{\sigma}{f_{cc}} \tag{11}$$

where ε_u is the ultimate strain, while f_{cc} is the cyclic compressive strength.

Each hysteresis cyclic loop is defined as in Section 1 and Fig. 1 by four characteristic points. The overall behavior of a concrete under cyclic loading is generally considered as a superposition of skeleton curves and unloading/loading branches. As previously mentioned, the skeleton curve pertaining to cyclic loading agrees well with the stress-strain relation under monotonic loading, therefore, the model proposed by Guo [48] and later extended by Xiao et al. [49] for monotonic loading is adopted in this study to describe the skeleton curve for EAFS concrete according to Eq. (12):

$$y = \begin{cases} px + (3-2p)x^2 + (p-2)x^3, 0 \le x < 1 \\ x/\left[q(x-1)^2 + x\right], x \ge 1 \end{cases} \tag{12}$$

where p and q are parameters that need to be determined experimentally. In this work, all specimens broke up in a brittle way when reaching the peak load, in such a way, the post-peak branch $x \ge 1$ is not visible and, hence, not discussed in this section. A comparison between the experimental and calculated skeleton curves is shown in Fig. 12 (the latter obtained with Eq. 12). Results show that the NAC theoretical curve agrees better with the experimental one than EAFS and BAR ones: this result is however expected by the authors because the original model was calibrated on traditional concrete only.

Once defined the skeleton curve, the strain of each characteristic point (x_u, x_r, x_c, x_e) must be defined to allow the description of the cyclic behavior. Before the peak point, the unloading curve is approximately linear and intersects the horizontal axis with a little residual strain. In such a way, the residual strain (x_r) can be defined based on the unloading strain (x_u) according to Eq. (13):

$$x_r = a x_u^b \tag{13}$$

where x_u is defined at priori when the model is applied. The intersection between the unloading and reloading curves, i.e. the common point, is related to unloading point according to Eq. (14):

$$x_c = c x_u + d \tag{14}$$

Concerning the end point, its value is related again to the unloading point with the same functional form as the residual point, according to Eq. (15):

$$x_e = g x_u^h \tag{15}$$

Table 8
Values of the parameters *a, b, c, d, g* and *h* obtained from experimental tests.

	a	*b*	*c*	*d*	*g*	*h*
NAC1	0.269	1.792	1.034	-0.051	1.221	1.063
EAF1	0.400	2.111	1.073	-0.062	1.253	0.995

Table 9
Values of the parameters *u, v, r* and *s* obtained from experimental tests.

	u	*v*	*r*	*s*
NAC1	1.0	1.3	1.0	0.9
EAF1	1.0	1.5	1.0	0.9

In Eqs. (13–15), the letters *a, b, c, d, g* and *h* indicate regression parameters that should be determined via calibration on the experimental data. Table 8 shows the values considered in this case for NAC1 and EAF1.

Once defined the characteristic points, the unloading and reloading curves can be obtained. According to Hu et al. [33], the unloading curve follows the expression in Eq. (16):

$$y = u \bullet y_u \left(\frac{x - x_r}{x_u - x_r}\right)^v \tag{16}$$

The reloading branch can be divided into two portions: the first connects the reloading to the common point, and the second is comprised between the common and end points. According to Eqs. (17–18), the first portion is assumed as a power function, while the second is linear:

$$y = r \bullet y_c \bullet \left(\frac{x - x_r}{x_c - x_r}\right)^s, x < x_c \tag{17}$$

$$y = \frac{y_e - y_c}{x_e - x_c} \bullet (x - x_c) + y_c, x \ge x_c \tag{18}$$

Again, *u, v, r* and *s* are parameters that need to be calibrated based on the experimental data, the results of such calibration are shown in Table 9.

Based on the above Eqs. (12–18), it is possible to define theoretically a complete stress-strain relation for a cyclic loading test. A validation of these equations is shown in Fig. 13 for a single loop: we have selected the last loop of the experimental loading history applied, which is

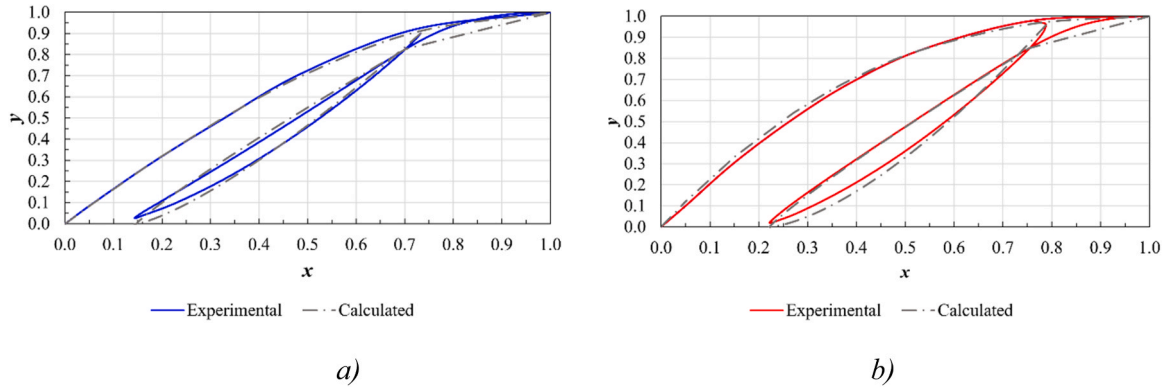

Fig. 13. Comparison between tested and calculated stress-strain relation in a loop of cyclic loading test for: a) NAC1; b) EAF1.

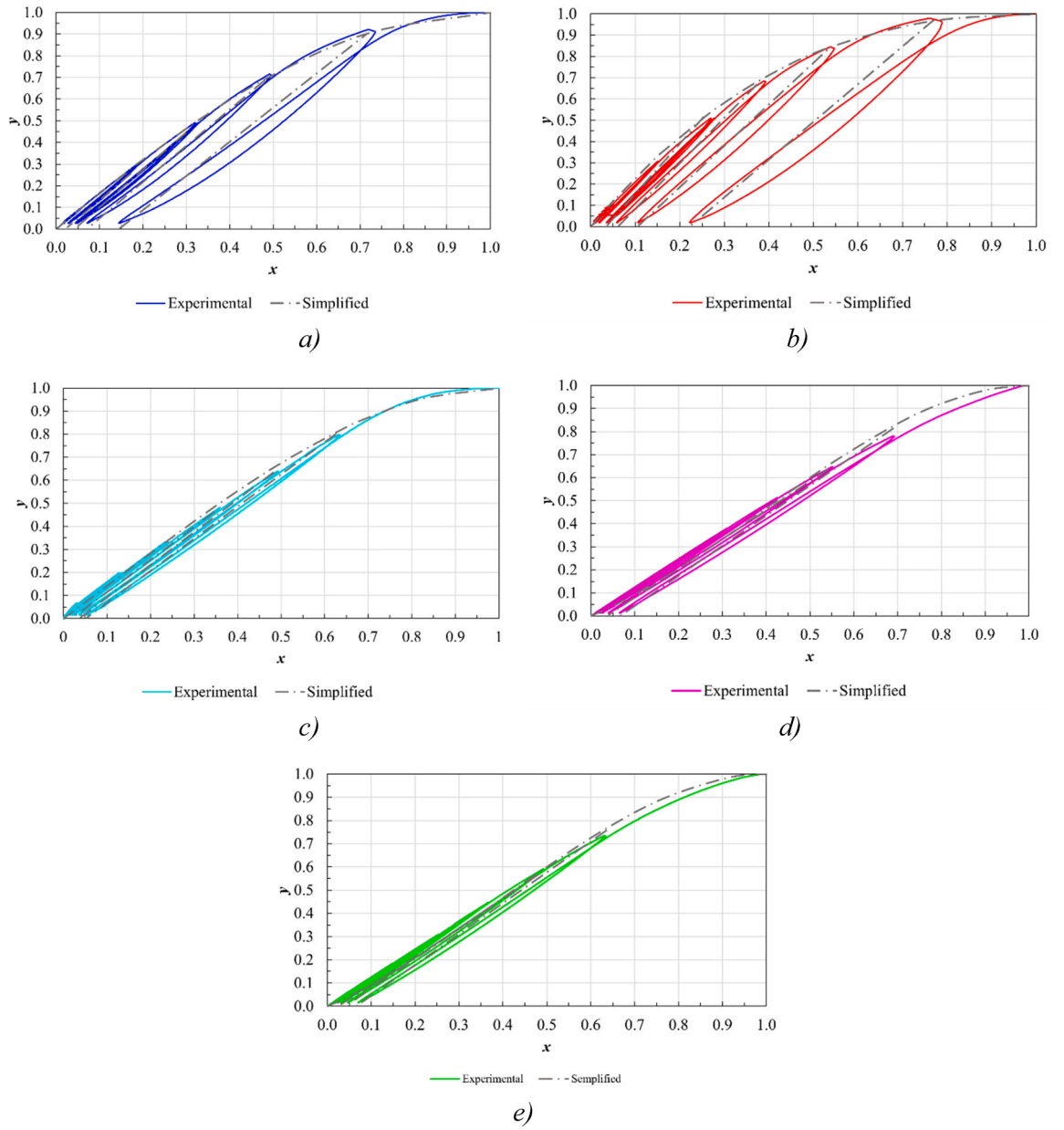

Fig. 14. Comparison between experimental and simplified stress strain relation for: a) NAC1; b) EAF1; c) NAC2; d) EAF2; e) BAR.

considered usually as the most difficult to be predicted due to presence of plastic deformations at high stress ranges. From Fig. 13 it is possible to observe how results are quite accurate, but the precision of the model is higher for NAC than for EAF. The agreement is particularly higher in the first portion of the reloading branch, conversely after the common point, the error is higher as a result of considering linear this portion of the curve.

4.2.2. Simplified model

The model shown at Section 4.2.1 to predict the full cyclic stress-strain behavior of NAC and EAFS concrete is characterized by a good agreement with the experimental data. However, it is quite complex, hence, its application may not always be convenient for engineering applications. A simplified approach consists in considering the unloading and reloading branches as linear and coincident, according to Eq. (19):

$$y = y_u \bullet \frac{x - x_r}{x_u - x_r} \tag{19}$$

As a completion, the skeleton curve is considered as previously defined in Eq. (12).

Fig. 14 shows a comparison between experimental data and the simplified stress-strain model proposed in this section. A satisfactory agreement is also shown in this case; hence the simplified model can be employed to describe the hysteresis behavior for NAC, EAFS and BAR concretes.

5. Conclusions

This work presents a comprehensive study on the cyclic behavior and deformative properties of concrete containing Electric Arc Furnace slags. The complete stress-strain relations under cyclic loading were discussed performing a comparison with conventional concrete. Tests were carried out both on specimens cured for a standard period of 28 days (short-term tests), and specimens which have six years (long-term tests) and were maintained from the date of casting in a protected environment. The deformative properties are calculated based on experimental data and a study on the evolution of damage is carried out. The constitutive models of the tested concretes under cyclic loading were analytically studied, and two models (a complete and one simplified) were proposed. According to the results obtained here, the following conclusions can be drawn:

- The strength gain is higher in EAFS concrete at early stages compared to those of NAC, whereas this strength enhancement remains more limited at prolonged times. However, the replacement of natural gravel with EAFS in concrete allows reaching higher strengths.
- Considering the cyclic loading protocol employed in this work, there is no influence in term of strength whether the specimens are subject to a cyclic or monotonic loading procedure, for any conglomerates tested here.
- The short-term tests show that the secant modulus is quite higher for EAFS concrete than for NAC at low stress levels, but there is a minimum difference when approaching the peak load. Differently, the long-term results demonstrate that EAFS concrete maintains a higher slope of the stress-strain curve than NAC independently from the applied stress level.
- Poisson's coefficient assumes a value in the range 0.20–0.30 for all the tested specimens until 0.8 f_c. A large scatter of data is recorded from 0.8 f_c.
- EAFS concrete is responsible for a more brittle behavior than NAC at failure, confirmed by higher values of normalized σ_{crit}/f_{cc}. Conversely, BAR concrete demonstrated the highest absolute values of volumetric strain during cyclic loading tests, because of the large deformative behavior of baritic aggregates.
- To predict the Elastic Modulus, the formulations EC2 and ACI2 are more accurate, but proper correction factors should be applied to consider the aggregate type. For the prediction of the stress-strain relation under cyclic loading, the constitutive relations proposed here afford a good estimate of the experimental data, both for NAC and EAFS concrete. A further simplified prediction is also possible, considering unloading and reloading branches as coincident and linear. This simplification does not lead to a sensible reduction of the prediction accuracy and thus is considered interesting for practical purposes.

CRediT authorship contribution statement

Mariano Angelo Zanini: Writing – original draft, Supervision, Project administration, Formal analysis, Conceptualization. **Vanesa Ortega-Lopez:** Writing – original draft, Validation, Supervision, Methodology, Formal analysis. **Daniel Trento:** Writing – original draft, Visualization, Investigation, Formal analysis, Data curation. **Flora Faleschini:** Writing – original draft, Supervision, Resources, Project administration, Methodology, Investigation, Funding acquisition, Formal analysis, Conceptualization.

Declaration of Competing Interest

The authors declare that they have no known competing financial interests or personal relationships that could have appeared to influence the work reported in this paper.

Data Availability

Data will be made available on request.

Acknowledgements

The authors would like to express their acknowledgement to Zerocento S.r.l. for providing the EAFS aggregate. This work received the DOR (Dotazione Ordinaria Ricerca) financing from the Department ICEA of the University of Padova.

References

[1] UN, A/RES/70/ACI1 – Transforming our world: the 2030 Agenda for Sustainable Development, 2015.
[2] G. Aid, D. Lazarevic, A. Kihl, Waste to resources: moving toward the 2030 sustainable development goals, in: Linnaneus Eco Tech 2016, Kalmar (Sweden), 21-23 November 2016, pp. 1-19.
[3] G.A. Blengini, E. Garbarino, S. Šolar, D.J. Shields, T. Hámor, R. Vinai, Z. Agioutantis, Life Cycle Assessment guidelines for the sustainable production and recycling of aggregates: the Sustainable Resource Management project (SARMa), J. Clean. Prod. 27 (2012) 177–181, https://doi.org/10.1016/j.jclepro.2012.01.020.
[4] B. Wang, L. Yan, Q. Fu, B. Kasal, A comprehensive review on recycled aggregate and recycled aggregate concrete, Resour. Conserv. Recycl. 171 (2021) 105565, https://doi.org/10.1016/j.resconrec.2021.105565.
[5] J. Ahmad, K.J. Kontoleon, A. Majdi, M.T. Naqash, A.F. Deifalla, N.B. Kahla, H. F. Isleem, S.M.A. Qaidi, A comprehensive review on the ground granulated blast furnace slag (GGBS) in concrete production, Sustainability 14 (2022) 8783, https://doi.org/10.3390/su14148783.
[6] S.C. Zago, F. Vernilli, O. Cascudo, The reuse of basic oxygen furnace slag as concrete aggregate to achieve sustainable development: characteristics and limitations, Buildings 13 (2023) 1193, https://doi.org/10.3390/buildings13051193.
[7] F. Faleschini, M.A. Zanini, C. De Martino, Design guidelines for structural and non-structural applications, in: F. Colagento, R. Cioffi, I. Farina (Eds.), Handbook of Sustainable Concrete and Industrial Waste Management, Woodhead Publishing, Cambridge, 2022, pp. 359–386.
[8] A. Santamaria, F. Faleschini, G. Giacomello, K. Brunelli, J.T. San José, C. Pellegrino, M. Pasetto, Dimensional stability of electric arc furnace slag in civil engineering applications, J. Clean. Prod. 205 (2018) 599–609, https://doi.org/10.1016/j.jclepro.2018.09.122.
[9] C. Pellegrino, F. Faleschini, Experimental database of EAF slag use in concrete, in: C. Pellegrino, F. Faleschini (Eds.), Sustainability Improvements in the Concrete

Industry: Use of Recycled Materials for Structural Concrete Production, Springer, 2016, pp. 141–175.
[10] J.M. Manso, J.J. Gonzalez, J.A. Polanco, Electric arc furnace slag in concrete, J. Mater. Civ. Eng. 16 (2004) 639–645, https://doi.org/10.1061/(ASCE)0899-1561(2004)16:6(639).
[11] C. Pellegrino, P. Cavagnis, F. Faleschini, K. Brunelli, Properties of concretes with black/oxidizing electric arc furnace slag aggregate, Cem. Concr. Compos. 37 (2013) 232–240, https://doi.org/10.1016/j.cemconcomp.2012.09.001.
[12] F. Faleschini, M.A. Fernandez-Ruiz, M.A. Zanini, K. Brunelli, C. Pellegrino, E. Hernandez-Montes, High performance concrete with electric arc furnace slag as aggregate: mechanical and durability properties, Constr. Build. Mater. 101 (2015) 113–121, https://doi.org/10.1016/j.conbuildmat.2015.10.022.
[13] N. Rojas, M. Bustamante, P. Muñoz, K. Godoy, V. Letelier, Study of properties and behavior of concrete containing EAF slag as coarse aggregate, Dev. Built Environ. 14 (2023) 100137, https://doi.org/10.1016/j.dibe.2023.100137.
[14] A.M. Rashad, Behavior of steel slag aggregate in mortar and concrete – a comprehensive overview, J. Build. Eng. 53 (2022) 104536, https://doi.org/10.1016/j.jobe.2022.104536.
[15] L.C.B. Costa, M.A. Nagueira, H.D. Andrade, J.M.F. de Carvalho, F.P. da Fonseca Elói, G.J. Brigolini, R.A.F. Peixoto, Mechanical and durability performance of concretes produced with steel slag aggregate and mineral admixtures, Constr. Build. Mater. 318 (2022) 126152, https://doi.org/10.1016/j.conbuildmat.2021.126152.
[16] I. Arribas, A. Santamaría, E. Ruiz, V. Ortega-López, J.M. Manso, Electric arc furnace slag and its use in hydraulic concrete, Constr. Build. Mater. 90 (2015) 68–79, https://doi.org/10.1016/j.conbuildmat.2015.05.003.
[17] F. Faleschini, M.A. Zanini, K. Toska, Seismic reliability assessment of code-conforming reinforced concrete buildings made with electric arc furnace slag aggregate, Eng. Struct. 195 (2019) 324–339, https://doi.org/10.1016/j.engstruct.2019.05.083.
[18] H.D. Andrade, J.M.F. de Carvalho, L.C.B. Costa, F.P. da Fonseca Elói, K.D. Do, Carmo e Silva, R.A.F. Peixoto, Mechanical performance and resistance to carbonation of steel slag reinforced concrete, Constr. Build. Mater. 298 (2021) 123910, https://doi.org/10.1016/j.conbuildmat.2021.123910.
[19] I. Sosa, C. Thomas, J.A. Polanco, J. Setién, J.A. Sainz-Aja, P. Tamayo, Durability of high-performance self-compacted concrete using electric arc furnace slag aggregate and cupola slag powder, Cem. Concr. Compos. 127 (2022) 104399, https://doi.org/10.1016/j.cemconcomp.2021.104399.
[20] A.-L. Beaucour, P. Pliya, F. Faleschini, R. Njinwoua, C. Pellegrino, A. Noumowé, Influence of elevated temperature on properties of radiation shielding concrete with electric arc furnace slag as coarse aggregate, Constr. Build. Mater. 256 (2020) 119385, https://doi.org/10.1016/j.conbuildmat.2020.119385.
[21] F. Faleschini, C. Pellegrino, Experimental behavior of reinforced concrete beams with electric arc furnace slag as recycled aggregate, Aci Mater. J. 110 (2013) 197–205.
[22] A. Santamaria, A. Garcia-Llona, V. Revilla-Cuesta, I. Piñero, V. Ortega-Lopez, Bending tests on building beams containing electric arc furnace slag as alternative binders and manufactured with energy-saving placement techniques, Structures 32 (2021) 1921–1933, https://doi.org/10.1016/j.istruc.2021.04.003.
[23] A. Santamaria, J.M. Romera, I. Marcos, V. Revilla-Cuesta, V. Ortega-López, Shear strength assessment of reinforced concrete components containing EAF steel slag aggregate, J. Build. Eng. 46 (2022) 103730, https://doi.org/10.1016/j.jobe.2021.103730.
[24] J.M. Lee, Y.J. Lee, Y.J. Jung, J.H. Park, B.S. Lee, K.H. Kim, Ductile capacity of reinforced concrete columns with electric arc furnace slag aggregate, Constr. Build. Mater. 162 (2018) 81–95, https://doi.org/10.1016/j.conbuildmat.2017.12.045.
[25] F. Faleschini, L. Hofer, M.A. Zanini, M. Dalla Benetta, C. Pellegrino, Experimental behavior of beam-column joints made with EAF concrete under cyclic loading, Eng. Struct. 139 (2017) 81–95, https://doi.org/10.1016/j.engstruct.2017.02.038.
[26] M.A. Zanini, Structural reliability of bridges realized with reinforced concretes containing electric arc furnace aggregates, Eng. Struct. 188 (2019) 305–319, https://doi.org/10.1016/j.engstruct.2019.02.052.
[27] B.P. Sinha, K.H. Gerstle, L.G. Tulin, Stress-strain relations for concrete under cyclic loading, J. Am. Concr. Inst. 61 (1964) 195–212.
[28] E. Chen, O. Buyukozturk, Constitutive model for concrete in cyclic compression, J. Eng. Mech. 111 (1985) 797–814, https://doi.org/10.1061/(ASCE)0733-9399(1985)111:6(797).
[29] J.B. Mander, M.J.N. Priestley, R. Park, Observed stress-strain behavior of confined concrete, J. Struct. Eng. 114 (1988) 1827–1849, https://doi.org/10.1061/(ASCE)0733-9445(1988)114:8(1827).
[30] J. Xiao, H. Li, Z. Yang, Fatigue behavior of recycled aggregate concrete under compression and bending loadings, Constr. Build. Mater. 38 (2013) 681–688, https://doi.org/10.1016/j.conbuildmat.2012.09.024.
[31] C. Thomas, J. Setién, J.A. Polanco, I. Lombillo, A. Cimentada, Fatigue limit of recycled aggregate concrete, Constr. Build. Mater. 52 (2014) 146–154, https://doi.org/10.1016/j.conbuildmat.2013.11.032.
[32] M. Breccolotti, A. D'Alessandro, F. Roscini, M.F. Bonfigli, Investigation of stress-strain behavior of recycled aggregate concrete under cyclic loads, Environ. Eng. Manag. J. 14 (2015) 1543–1552.
[33] X. Hu, Q. Lu, Z. Xu, W. Zhang, S. Cheng, Compressive stress-strain relation of recycled aggregate concrete under cyclic loading, Constr. Build. Mater. 52 (2018) 146–154, https://doi.org/10.1016/j.conbuildmat.2018.10.137.
[34] B. Gonzalez-Fonteboa, F. Martinez-Abella, J. Eiras-Lopez, S. Seara-Paz, Effect of recycled coarse aggregate on damage of recycled concrete, Mater. Struct. 44 (2011) 1759–1771, https://doi.org/10.1617/s11527-011-9736-7.
[35] B. Gonzalez-Fonteboa, F. Martinez-Abella, M.F. Herrador, S. Seara-Paz, Structural recycled concrete: Behaviour under low loading rate, Constr. Build. Mater. 28 (2012) 111–116, https://doi.org/10.1016/j.conbuildmat.2011.08.010.
[36] S.P. Shah, S. Chandra, Critical stress, Volume Change, and Microcracking of Concrete, Acids J. Proc. 65 (1968) 770–780.
[37] D. Zhang, Q. Li, L. Wang, A microscopic approach to rate effect on compressive strength of concrete, Eng. Fract. Mech. 72 (2005) 2316–2327, https://doi.org/10.1016/j.engfracmech.2005.01.012.
[38] J.A. Carneiro, P.R.L. Lima, M.B. Leite, R.D.T. Filho, Compressive stress-strain behavior of steel fiber reinforced-recycled aggregate concrete, Cem. Concr. Compos. 46 (2014) 65–72, https://doi.org/10.1016/j.cemconcomp.2013.11.006.
[39] A.Y. Elghazouli, D.V. Bompa, B. Xu, A.M. Ruiz-Teran, P.J. Stafford, Performance of rubberized reinforced concrete members under cyclic loading, Eng. Struct. 166 (2018) 526–545, https://doi.org/10.1016/j.engstruct.2018.03.090.
[40] B.P. Sinha, K.H. Gerstle, L.G. Tulin, Stress-Strain Relations for Concrete Under Cyclic Loading, Acids J. Proc. 61 (1964) 195–211.
[41] S.P. Shah, G. Winter, Inelastic behavior and fracture of concrete, Acids J. Proc. 63 (1966) 925–930.
[42] I.D. Karsan, J.O. Jirsa, Behavior of concrete under compressive loadings, ASCE J. Struct. Eng. 95 (1969) 2543–2563, https://doi.org/10.1061/JSDEAG.0002424.
[43] B.Y. Bahn, C.T. Hsu, Stress-Strain Behavior of Concrete under Cyclic Loading, Acids Mater. J. 95 (1988) 178–193.
[44] D. Palermo, F.J. Vecchio, Compression Field Modeling of Reinforced Concrete Subjected to Reversed Loading: Formulation, Acids Struct. J. 100 (2003) 616–625.
[45] J.F. Sima, P. Roca, C. Molins, Cyclic constitutive model for concrete, Eng. Struct. 30 (2008) 695–706, https://doi.org/10.1016/j.engstruct.2007.05.005.
[46] F. Aslani, S. Nejadi, Cyclic constitutive model for high-strength concrete confined by ultra-high-strength and normal-strength transverse reinforcements, Aust. J. Struct. Eng. 12 (2012) 159–172, https://doi.org/10.7158/13287982.2011.11465088.
[47] F. Aslani, R. Jowkarmeimandi, Stress-strain model for concrete under cyclic loading, Mag. Concr. Res. 64 (2012) 673–685, https://doi.org/10.1680/macr.11.00120.
[48] Z.H. Guo, Strength and Deformation of Concrete: Experimental basis and Constitutive Relations, Tsinghua University Press, Beijing, 1997.
[49] J. Xiao, J. Li, C. Zhang, Mechanical properties of recycled aggregate concrete under uniaxial loading, Cem. Concr. Res. 35 (2005) 1187–1194, https://doi.org/10.1016/j.cemconres.2004.09.020.
[50] H. Yang, J. Fang, J. Jiang, M. Li, J. Mei, Compressive stress-strain curve of recycled concrete under repeated loading, Constr. Build. Mater. 387 (2023) 131598, https://doi.org/10.1016/j.conbuildmat.2023.131598.
[51] EN 197-1:2011, Cement - Part 1: Composition, specification and conformity criteria for common cements, European Committee for Standardization, Brussels, 2011.
[52] B. Pomaro, F. Gramegna, R. Cherubini, V. De Nadal, V. Salomoni, F. Faleschini, Gamma-ray shielding properties of heavyweight concrete with Electric Arc Furnace slag as aggregate: An experimental and numerical study, Constr. Build. Mater. 200 (2019) 188–197, https://doi.org/10.1016/j.conbuildmat.2018.12.098.
[53] C. Pellegrino, V. Gaddo, Mechanical and durability characteristics of concrete containing EAF slags as aggregate, Cem. Concr. Compos. 31 (2009) 663–671, https://doi.org/10.1016/j.cemconcomp.2009.05.006.
[54] CEN, EN 1097-6:2022, Tests for mechanical and physical properties of aggregates - Part 6: Determination of particle density and water absorption, European Committee for Standardization, Brussels, 2022.
[55] CEN, EN 12390-3:2019, Testing hardened concrete - Part 3: Compressive strength of test specimens, European Committee for Standardization, Brussels, 2019.
[56] CEN, EN 12390-6:2009, Testing hardened concrete - Part 6: Tensile splitting strength of test specimens, European Committee for Standardization, Brussels, 2009.
[57] CEN, EN 12350-2:2019, Testing fresh concrete - Part 2: Slump test, European Committee for Standardization, Brussels, 2019.
[58] CEN, EN 206-1:2013, Concrete - Part 1: Specification, performance, production and conformity, European Committee for Standardization, Brussels, 2013.
[59] M.F.M. Zain, H.B. Mahmud, A. Ilham, M. Faizal, Prediction of splitting tensile strength of high-performance concrete, Cem. Concr. Res. 32 (2002) 1251–1258, https://doi.org/10.1016/S0008-8846(02)00768-8.
[60] S. Bhanja, B. Sengupta, Influence of silica fume on the tensile strength of concrete, Cem. Concr. Res. 35 (2005) 743–747, https://doi.org/10.1016/j.cemconres.2004.05.024.
[61] D. Wu, Y. Yu, Z. Chen, X. Zhao, Shape effect on compressive mechanical properties of compound concrete containing demolished concrete lumps, Constr. Build. Mater. 187 (2018) 50–64, https://doi.org/10.1016/j.conbuildmat.2018.07.086.
[62] CEN, EN 1992-1-1, Eurocode 2: Design of concrete structures – Part 1.1: General rules and rules for buildings, European Committee for Standardization, Brussels, 2004.
[63] P. Sukontasukkul, P. Nimityongskul, S. Mindess, Effect of loading rate on damage of concrete, Cem. Concr. Res. 34 (2004) 2127–2134, https://doi.org/10.1016/j.cemconres.2004.03.022.
[64] L. Rondi, G. Bregoli, S. Sorlini, L. Cominoli, C. Collivignarelli, G. Plizzari, Concrete with EAF steel slag as aggregate: A comprehensive technical and environmental characterization, Compos. Part B: Eng. 90 (2016) 195–202, https://doi.org/10.1016/j.compositesb.2015.12.022.
[65] S. Kilincarslan, I. Akkurt, C. Basyigit, The effect of barite rate on some physical and mechanical properties of concrete, Mater. Sci. Eng.: A 424 (2006) 83–86, https://doi.org/10.1016/j.msea.2006.02.033.

[66] ACI 318-19, Building Code Requirements for Structural Concrete and commentary, American Concrete Institute, Farmington Hills (MI, USA), 2019.
[67] M.A. Farooq, Y. Sato, T. Ayano, K. Niitani, Experimental and numerical investigation of static and fatigue behavior of mortar with blast furnace slag sand as fine aggregates in air and water, Constr. Build. Mater. 143 (2017) 429–443, https://doi.org/10.1016/j.conbuildmat.2017.03.147.
[68] M.A. Farooq, Y. Sato, K. Niitani, Experimental investigation of monotonic behavior and stress-strain models of AE and non-AE high strength concrete with BFS fine aggregates under freezing and thawing, Constr. Build. Mater. 249 (2020) (2020) 118679, https://doi.org/10.1016/j.conbuildmat.2020.118679.